Supplementary Information: Underpinning hybridization intuition for complex nanoantennas by magnetoelectric quadrupolar polarizability retrieval

Felipe Bernal Arango,* Toon Coenen, and A. Femius Koenderink

AMOLF, Center for Nanophotonics, FOM Institute AMOLF,Science Park 104, 1098 XG Amsterdam, The Netherlands

E-mail: bernal@amolf.nl

January 14, 2014

Quadrupolar fields and 12×12 α^S-tensor

Here we show that given the choice of casting the rank 2 quadrupole tensor in a vector, and reducing redundancy due to the tensor symmetry, the $\diamond$ operator is completely determined. Starting from the symmetric traceless quadrupole tensor Q, the field emitted by a quadrupole in Einstein notation is

$$E_i(\mathbf{r}) = \frac{\omega^2 \mu\mu_0}{3!} Q_{jk} \nabla'_k \mathbf{G}_{ji}(\mathbf{r}, \mathbf{r}'), \tag{1}$$

with ω the optical frequency, $\mu\mu_0$ the permeability of the surrounding medium and G the $3\times$ 3 electric Green dyadic. That the tensor Q_{ij} is symmetric allows a regrouping of terms

*To whom correspondence should be addressed

(where we abbreviate $\partial_{x'}\mathbf{G}_{ij}(\mathbf{r},\mathbf{r'})$ as $G_{ijx'}$)

$$\mathbf{E} = \frac{\omega^2\mu\mu_0}{3!}\begin{pmatrix} Q_{12}(G_{11y'}+G_{12x'})+Q_{13}(G_{11z'}+G_{13x'})+Q_{23}(G_{12z'}+G_{13y'})+Q_{11}G_{11x'}+Q_{22}G_{12y}+Q_{33}G_{13z'} \\ Q_{12}(G_{21y'}+G_{22x'})+Q_{13}(G_{21z'}+G_{23x'})+Q_{23}(G_{22z'}+G_{23y'})+Q_{11}G_{21x'}+Q_{22}G_{22y}+Q_{33}G_{23z'} \\ Q_{12}(G_{31y'}+G_{32x'})+Q_{13}(G_{31z'}+G_{33x'})+Q_{23}(G_{32z'}+G_{33y'})+Q_{11}G_{31x'}+Q_{22}G_{32y}+Q_{33}G_{33z'} \end{pmatrix} \tag{2}$$

which can be identified as

$$\mathbf{E} = \frac{\omega^2\mu\mu_0}{3!}(\diamond'\overline{\mathbf{G}}^{\top}(\mathbf{r},\mathbf{r'}))^{\top}\cdot\mathbf{Q}. \tag{3}$$

Thereby defining $\mathbf{Q}$ as a 6-vector as in the main manuscript fixes the definition of $\diamond$. Mutatis mutandi the same reasoning holds if in Eq. (2) one eliminates Q_{zz} on basis of the traceless nature of the tensor Q, in which case inserting the definition of $\hat{\mathbf{Q}}$ fixes $\hat{\diamond}$.

Dolmen α^S-tensor elements

To complement our report in the main manuscript of elements of $|\alpha^S|$ at one wavelength and as a logarithmic color scale for the silver dolmen, here we report the superpolarizability tensor element amplitude and phase versus wavelength grouped in three figures, i.e. Fig.1,2 and 3.

Gold disk α^S-tensor elements

To complement our report in the main manuscript of elements of $|\alpha^S|$ at one wavelength and as a logarithmic color scale for the Au nanodisk on a Si substrate, here we report the superpolarizability tensor element amplitude and phase versus wavelength in Fig.4.

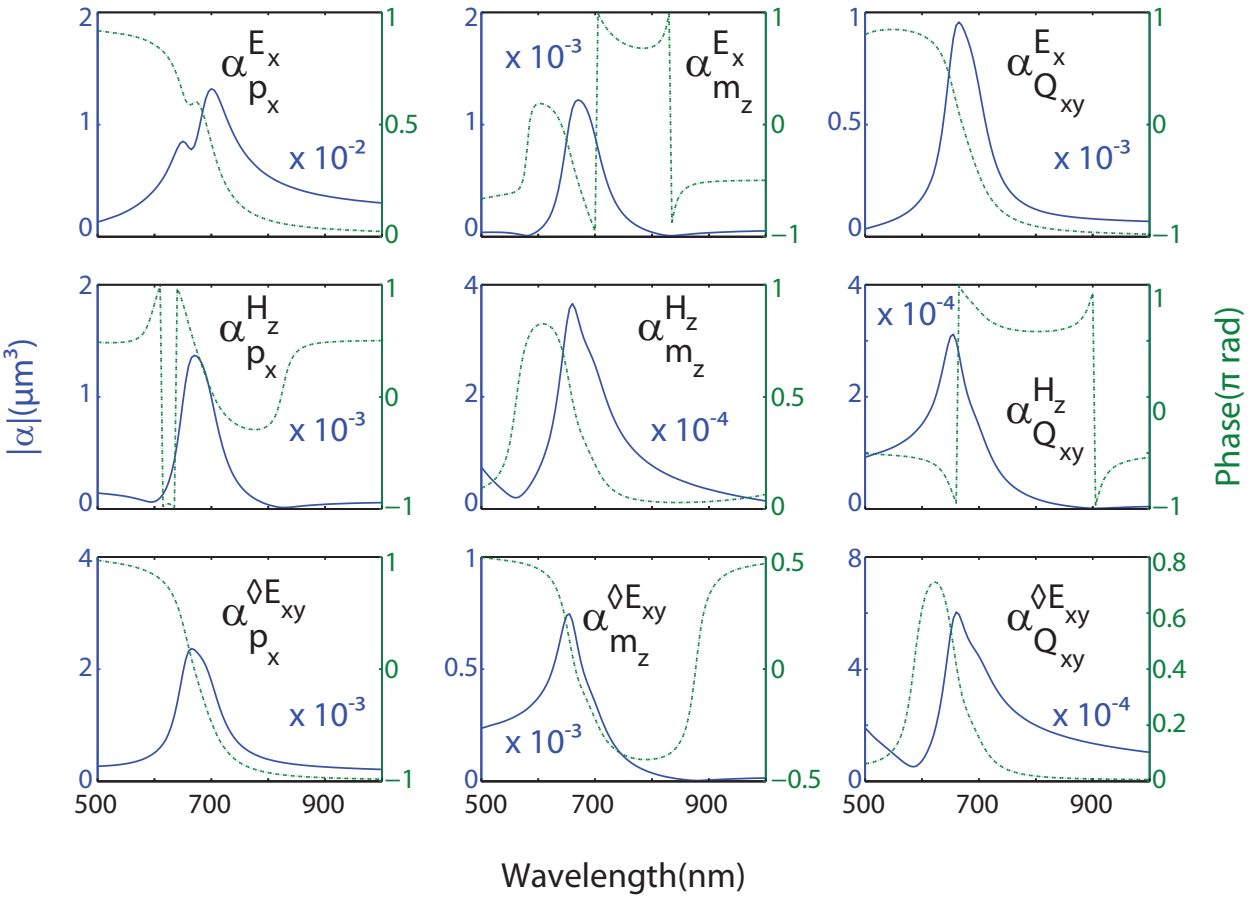

Figure 1: Elements related to p_x, m_z and $Q_{x,y}$ of the α^S-tensor of a silver dolmen structure. These elements span the subspace relevant for PIT in the dolmen system. Solid curves show amplitude while dashed curves show phase.

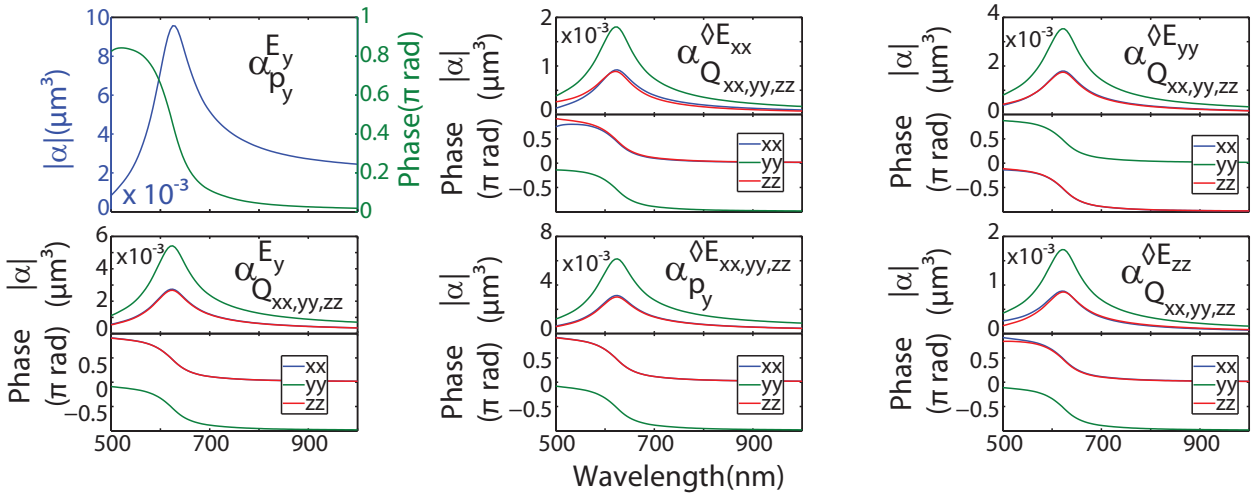

Figure 2: Elements related to p_y and $Q_{xx,yy,zz}$ of the α^S-tensor of a silver dolmen structure. These elements correspond to excitation of the symmetric dimer resonant mode, which has a strong electric dipole character, as well as carrying a linear y-oriented quadrupole moment.

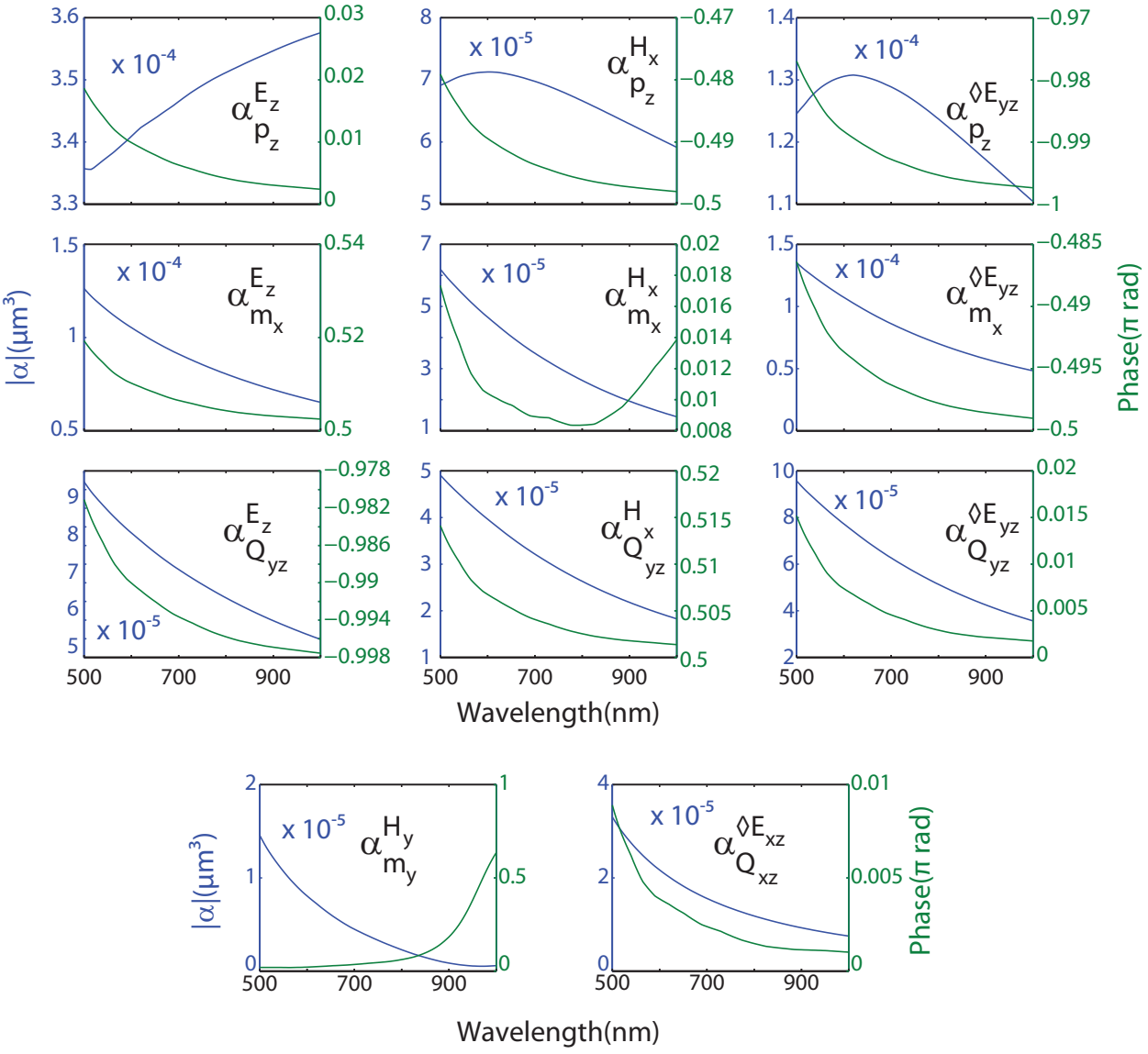

Figure 3: Summary of weaker elements of the α^S-tensor of the silver dolmen structure, generally corresponding to out-of-plane charge separation.

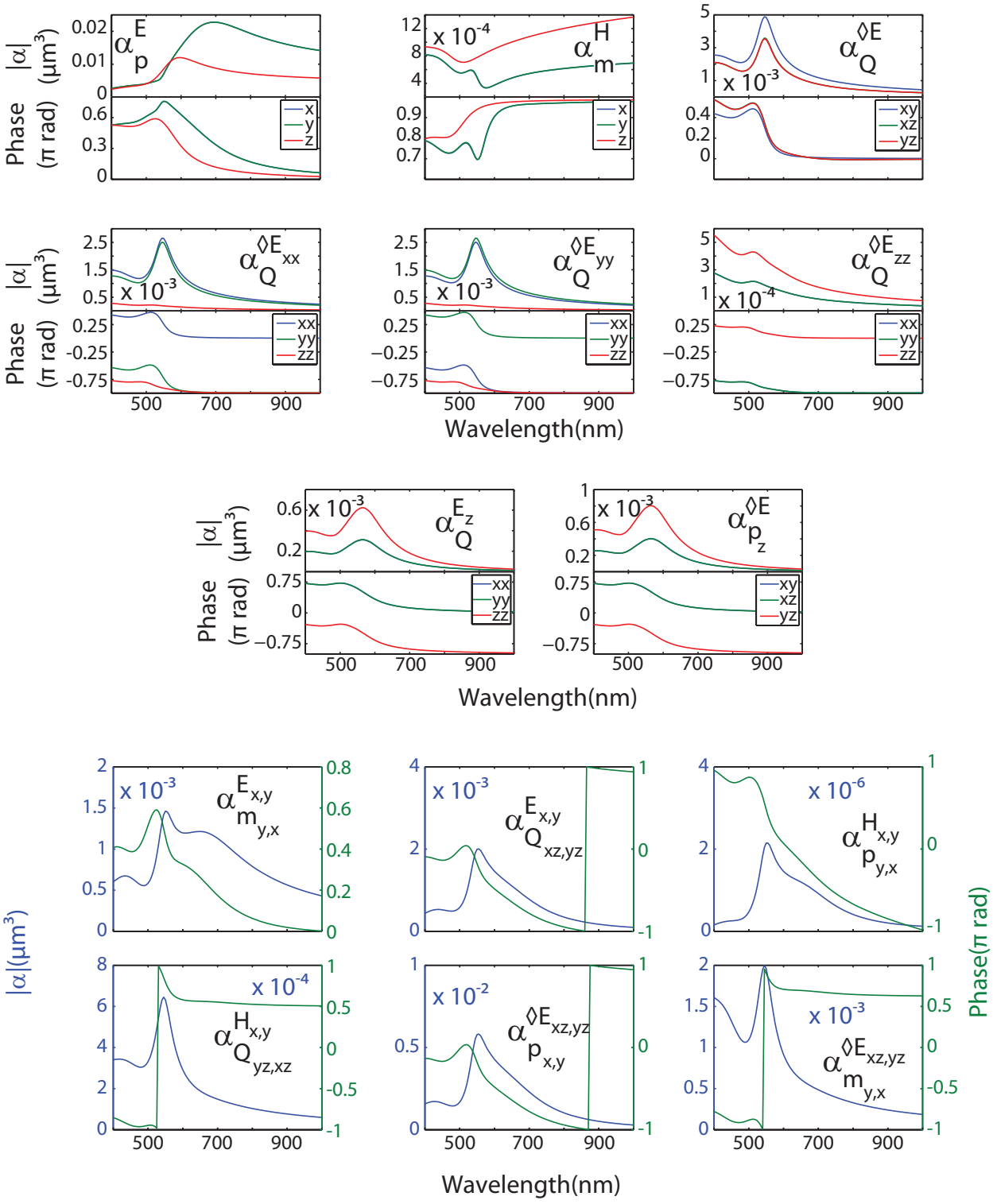

Figure 4: Elements of the α^S-tensor of a gold cylinder with 180 nm diameter and 80 nm height.